Applied Radiation and Isotopes 70 (2012) 643–649

Contents lists available at SciVerse ScienceDirect

Applied Radiation and Isotopes

journal homepage: www.elsevier.com/locate/apradiso

On the use of a (^{252}Cf–^{3}He) assembly for landmine detection by the neutron back-scattering method

N. Elsheikh [a,*], G. Viesti [b], I. ElAgib [c], F. Habbani [d]

[a] College of Applied & Industrial Science, Department of Physics, University of Juba, Khartoum, P.O. Box 12327/1, Sudan
[b] Dipartimento di Fisica ed Astronomia dell' Universita di Padova, Via Marzolo 8, I-35131 Padova, Italy
[c] College of Science, King Saud University, P.O. Box 2455, Saudi Arabia
[d] Faculty of Science, Physics Department, University of Khartoum, Khartoum, P.O. Box 321, Sudan

ARTICLE INFO

Article history:
Received 17 July 2011
Received in revised form
3 October 2011
Accepted 7 January 2012
Available online 18 January 2012

Keywords:
Neutron back-scattering technique
Landmine detection
^{252}Cf–^{3}He assembly

ABSTRACT

Experiments were carried out to optimize the performance of the neutron back-scattering (NBS) technique in landmine detection using an assembly consisting of three different layers placed above a ^{252}Cf neuron source, producing about 10^4 s^{-1}, in conjunction with a ^{3}He detector. The assembly was optimized experimentally. The selected assembly configuration was then examined against different ^{252}Cf stand-off distances and mine burial depths using dummy landmines. Furthermore, Monte Carlo simulations were performed to study the effect of the shield when a ^{252}Cf source in the range 10^4–10^7 s^{-1} was employed, and to optimize the geometry for future prototypes.

1. Introduction

In the currently de-mining operation, the suspect point is determined by the metal detector search. The suspect point is then manually tested using usually rigid metal stick of about 250 mm length to determine the correct position and shape of the buried object before any attempt to bring it to the soil surface. In this procedure, the risk of mine explosion, requires a time consuming slow operation. The process is slow, dangerous and laborious. Although metal detectors are very efficient in finding mines that contain metal parts, they have problems in finding nearly metal-free mines (Sieber, 1998). Consequently it is highly significant to verify possible alternative techniques for detection of low-metal landmines, searching for the most simple and straightforward method to complement the commonly used metal detectors.

The most common explosives used in landmines are TNT ($C_7H_5N_3O_6$) and RDX ($C_3H_6N_6O_6$). The anti-personnel landmines (APMs) are usually designed in the form of a disk or a cylinder, with diameters from 20 to 125 mm, lengths from 50 to 100 mm, with a mass as little as 30 g, while anti-tank landmines (ATMs) often have the shape of truncated cylinders or squares with round corners, with largest dimensions from 150 to 300 mm and thicknesses from 50 to 90 mm. Landmines are buried at various depths from the surface, at a maximum depth of about 50 mm for APMs and greater than 150 mm for ATMs (Hussein and Waller, 2000).

Nuclear-based methods, particularly those applying thermal or fast neutron-induced γ-ray emission, are useful because the major constituent elements of the explosives such as hydrogen, oxygen, carbon and nitrogen vastly differ in their modes of interaction with neutrons, allowing the determination of a suspect concentration of a given element, due to the explosive material, that differs from the one in the soil. Moreover, the low detection limits obtained by nuclear-based methods are generally well within the requirements of the present application.

Thermal neutron and fast neutron analysis have been proposed for landmine detection (Cinausero et al., 2004; Lunardon et al., 2004; McFee et al., 1998; Cousins et al., 1998; Kuznetsov et al., 2004; Vourvopoulos and Womble, 2001) looking at the characteristic gamma-rays produced by neutrons. However, one of the major limitations in the use of such sensors is represented by their weight and size that makes them usable only in vehicle-mounted systems, with a specific limited impact on the humanitarian de-mining operations (Viesti et al., 2006).

On the other hand, one of the proposed nuclear techniques to detect non-metallic landmines that has successfully been used in prototypes hand-held systems is the neutron back-scattering (NBS) method (Bom et al., 2004; Borgonovi et al., 2000; Brooks and Drosg, 2005; Csikai et al., 2004; Datema et al., 2000, 2002; Kiraly et al., 2001). This technique is based on the use of a radionuclidic neutron source such as ^{252}Cf to irradiate the soil.

* Corresponding author. Tel.: +249 906082101.
E-mail address: nassreldeen.elsheikh@yahoo.com (N. Elsheikh).

0969-8043/$ - see front matter © 2012 Elsevier Ltd. All rights reserved.
doi:10.1016/j.apradiso.2012.01.004

The yield of thermalized back-scattered neutrons depends mainly on the hydrogen content in the irradiated volume. Therefore, to confirm the presence of the mine, a NBS sensor will verify the presence of a hydrogenous anomaly in the target point. However, soil moisture content impacts the effectiveness of the NBS sensor. The landmine can be detected only when the thermalization capability of the buried mine is significantly greater than that of the surrounding soil, the latter being essentially due to the soil moisture. A specific analysis of this problem, reported by Obhadas et al. (2004), led to the conclusion that the best use of the NBS method is in countries where the soil moisture is generally lower than 10%, this condition being valid in the case of arid soils. Generally, due to the isotropy of the radioactive sources, only a fraction of the emitted fast neutrons is irradiating the object region, i.e. the portion of the soil surface to be explored is determined by the acceptance of the detection system. The majority of the emitted neutrons normally generate background on the materials around the detectors and on the detectors themselves. The demands of protecting the operator from neutron dose from the one hand and of reducing the background due to the source neutrons that hit directly the detector on the other hand, represent the major challenges in bringing the NBS technique in field use.

On the basis of such considerations, experiments have been carried out to optimize the performance of the NBS method for landmine detection in dry soils by designing an effective shield assembly above a suitable ^{252}Cf source–^{3}He detector system.

The laboratory measurements were followed by Monte-Carlo simulations first close to the geometry of the experiment and then to study the capabilities of this landmine detector system in the presence of a stronger ^{252}Cf source and to optimize its design in view of a future prototype.

2. Experimental measurements

A sealed ^{252}Cf neutron source from Isotope Products Laboratories (USA) producing about 0.7×10^{4} s^{-1} that was employed in this wok, was placed 2 cm above the soil. The neutron emission, estimated from the original source activity at the date of delivery was supposed to be known with an uncertainty of $-10\%+20\%$. The detector used was ^{3}He proportional counter ASPECT SN-01, filled with a gas mixture (284 kPa ^{3}He+121 kPa Ar+2.7 kPa CO_2), having an effective length of 40 cm and diameter of 3 cm. The detector was placed typically at 5 cm over the soil and 5 cm away from the source.

Two dummy landmines were employed in this work. The first is the IAEA standard dummy anti-personnel landmine DLM2 (Brooks et al., 2004) that consisted of 100 g of a TNT simulant sealed in a cylindrical acrylic container of mass 100 g, diameter 80 mm and height 34 mm.

The second dummy ATM consisted of 2000 g melamine sealed in a polyvinyl chloride container of thickness 1 cm, diameter 23 cm and height 6 cm.

The shield consisted of three layers located above the ^{252}Cf–^{3}He assembly and centered on the ^{252}Cf position. The first is a plexiglass box of dimensions 38 cm × 18 cm × 5 cm filled by boric acid powder (H_3BO_3) of thickness 2 cm and mass 1.72 kg. The boric acid was used as an absorber to protect the operator from neutron irradiation.

This layer was fixed on top of a 39 cm × 19 cm × 4 cm graphite block of mass 5 kg, contained in aluminum box of 40 cm × 20 cm × 12 cm, representing the second layer. The graphite was employed as a reflector to increase the neutron flux density directed towards the soil.

The third layer consisted of a copper box of dimensions 35 cm × 9 cm × 0.5 cm filled by a gadolinium oxide powder (Gd_2O_3). It has a mass of 0.45 kg and is fixed, when needed, on the bottom of the aluminum box, above the ^{3}He detector. The gadolinium oxide was employed to reduce the detector background due to the thermal neutrons coming back from the (graphite+boric acid) assembly. The shield was located at 10 cm over the soil. A photograph of the set-up used for the tests is shown in Fig. 1.

As mentioned above the NBS systems for landmine detection have been reported by others. For example, the system used by Datema et al. (2002) employed a ^{252}Cf neutron source and carbon and borated paraffin as a neutron reflector and absorber, respectively. To reduce the count rate due to thermal neutrons coming back from the paraffin, they placed a cadmium layer around the detector and source.

In this work, boric acid was used as a shielding material and cadmium was replaced by gadolinium oxide layer. The replacement of cadmium is due to the high energy prompt gamma radiation (9.1 MeV) expected from the reaction ^{113}Cd(n,γ)^{114}Cd (Reines and Cowan, 1953) which requires the need of a heavy gamma shielding material, thus affecting the portability of the

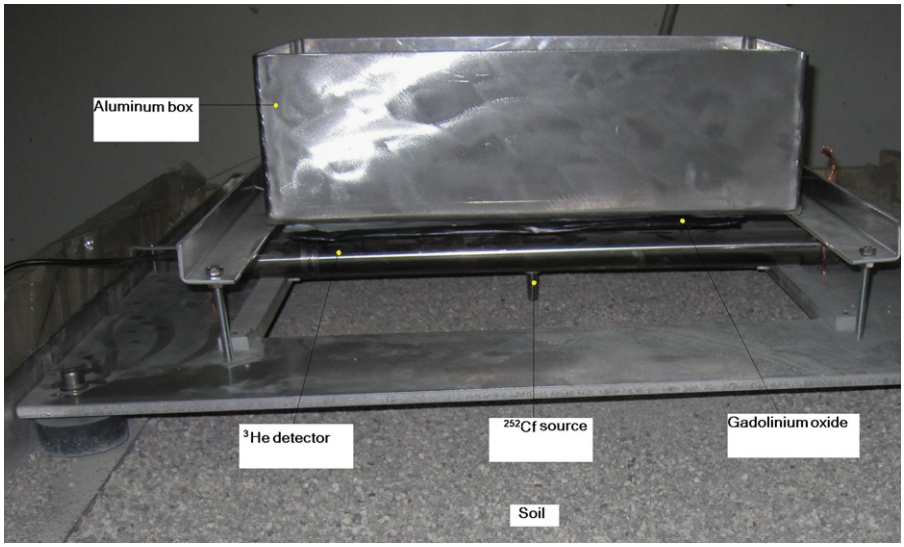

Fig. 1. A photograph for the experimental set-up.

device. On the other hand, the energy of the prompt gamma radiation emitted from the gadolinium thermal neutron capture reaction $^{157}Gd(n,\gamma)^{158}Gd$, was evaluated with Monte Carlo calculation within our proposed layer dimensions and found to be 1.9 MeV. In addition, the absorption cross section for thermal neutrons of gadolinium (about 255900 b) is much higher than that of cadmium (about 20784 b). Furthermore, ^{157}Gd is present in natural gadolinium with an abundance of 15.7%, which is larger than 12.3% for ^{113}Cd in natural cadmium (D'Mellow et al., 2007).

The test measurements were made using a laboratory test bed of dry sand of 150 cm × 80 cm area and a depth of 50 cm. The signal output from the ^{3}He detector was processed by an amplifier–discriminator unit and the filtered pulse height was fed to a multi-channel analyzer hosted in a desktop computer. Among many parameters, the detection efficiency of the ^{3}He-filled proportional counter relies on its sensitivity to slow neutrons.

The reaction for conversion of slow neutrons into directly detectable particles in the ^{3}He-filled proportional counter is $^{3}He(n,p)^{3}H$.

The thermal neutron cross section for this reaction is 5330 b, and its value drops rapidly with increasing neutron energy and is proportional to $1/\upsilon$ over much of the range, where υ is the neutron velocity (Knoll, 1989). This fact ensures that this detector is practically insensitive to direct fast neutrons emitted from the ^{252}Cf source and confirms the practicality of using ^{3}He detector in our current measurements.

Due to the weakness of the source used in this work (about $10^{4}\ s^{-1}$) and the need for sufficient statistics, the acquisition time for all measurements was chosen to be 20 min.

The shielded ^{252}Cf–^{3}He assembly detects the landmine simulant by monitoring the difference in counts in the presence and absence of the buried landmine, respectively, as the shielded source–detector system is scanned across the object.

The results are reported in terms of variations in signal-to-background ratio (S/B) due to changes in detector position and net counts $(I-I_o)$ as a function of reflector thickness, source height, mine depth and device location.

The net counts $(I-I_o)$ were determined by subtracting from the measured counts with landmine in soil, I, the ones measured without the landmine, I_o, while the signal-to-background ratio was determined as

$$S/B = [(I-I_o)/I_o] \times 100$$

3. Experimental results

The measurements were started by optimizing firstly the relative distance between the detector and the ^{252}Cf source, by measuring the average counts while locating the detector at different positions i.e. $X = \pm 2, \pm 3, \pm 4$ and ± 5 cm away from the source. The signal-to-background ratio was then calculated and averaged for measurements taken at a given distance at both sides of the source. The results reported in Fig. 2 show that the signal-to-background ratio increases with distance up to the position $X=5$ cm, due to the lowest background measured at this point. After this observation, the detector was located at 5 cm from the source for the next measurements.

The graphite reflector thickness was then optimized by measuring the neutron net counts due to back-scattered ^{252}Cf neutrons rate from both APM and ATM alternatively while increasing the reflector thickness in the range $t=2$–6 cm, to determine the optimum operating condition.

As presented in Fig. 3, the net counts increased with the reflector thickness, reaching the maximum at $t=6$ cm. However, allowing for the portability of the detection system, 4 cm was considered a reasonable reflector thickness.

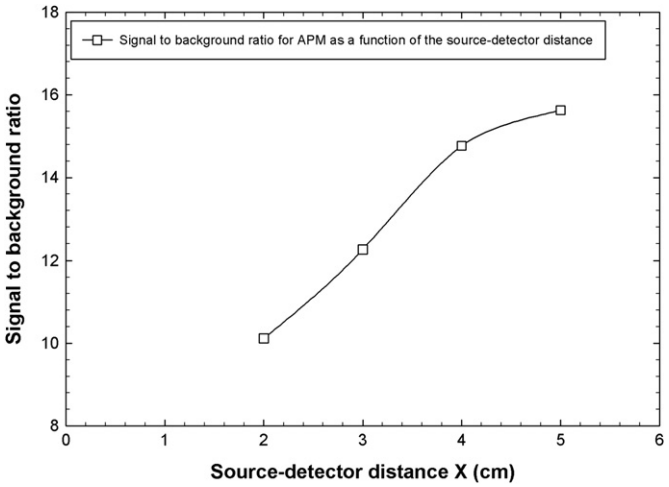

Fig. 2. Variation of signal to background ratio with the source–detector distance.

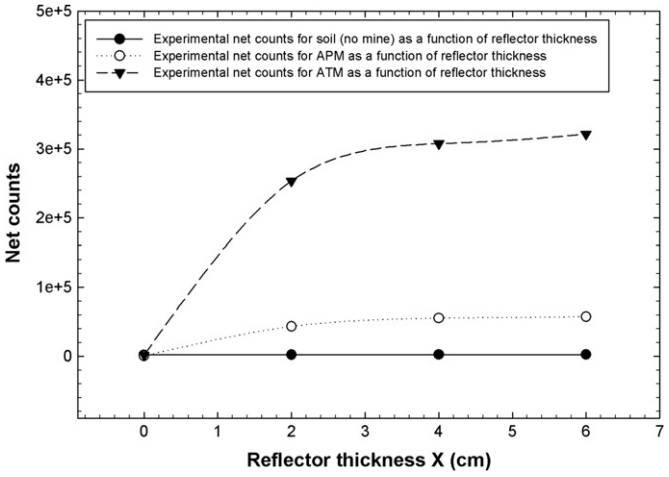

Fig. 3. Net counts measured as a function of the reflector thickness.

In order to evaluate the effectiveness of the boric acid layer in protecting the operator, the average equivalent dose rate for neutrons was measured using a Berthold LB 6411 Neutron Dose Rate Detector at different shield configurations, with a neutron standard dosimeter fixed at 15 cm above the aluminum box and at 35 cm away from the source.

As shown in Fig. 4, the average dose rate corresponding to the best configuration (2 cm boric acid + 4 cm carbon reflector) was found to be 0.5 μSv/h for the above mentioned position. Further increase of the reflector thickness does not decrease the measured dose.

To study the feasibility of using the gadolinium oxide layer for reducing the background due to the thermal neutrons coming back from the boric acid, the background was recorded at each configuration for the reflector thickness + boric acid layers, with and without the gadolinium oxide layer.

As shown in Fig. 5, at the best configuration for the reflector + boric acid assembly, the gadolinium oxide layer has effectively reduced the total background by 13.5%. It is worth noting that the length of this layer (35 cm) is shorter than that of the ^{3}He detector (40 cm). Consequently a better background reduction is expected when the gadolinium oxide layer is lengthened to completely cover the detector.

Finally, to determine the optimal operating conditions, the final shield configuration (2 cm boric acid + 4 cm carbon + 0.5 cm gadolinium oxide) was examined against different ^{252}Cf stand-off

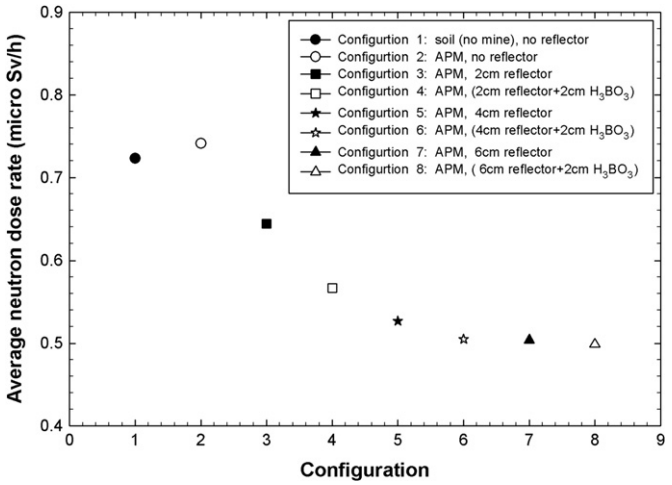

Fig. 4. Equivalent dose rate for different shield configurations.

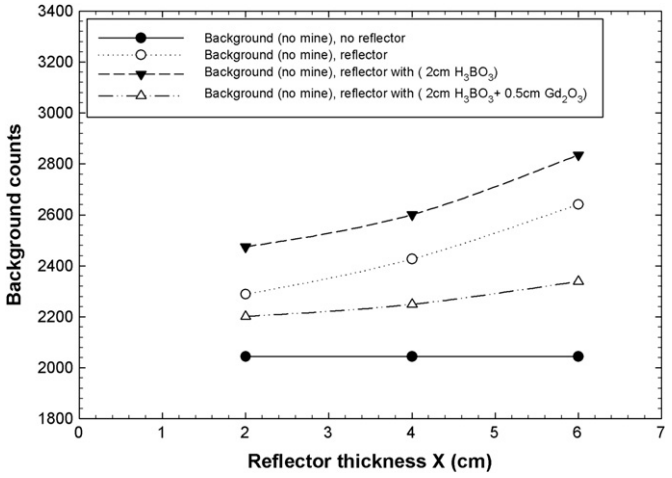

Fig. 5. Variation of background counts with different shield configurations.

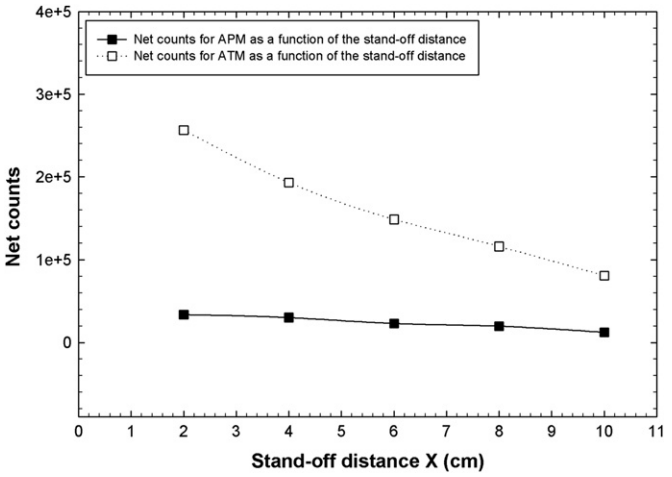

Fig. 6. Net counts distribution as function of stand-off distance for both APM and ATM.

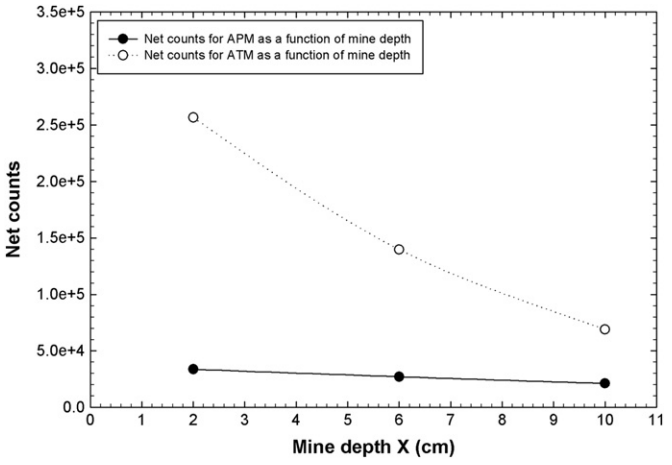

Fig. 7. Net counts distribution as a function of mine depth for APM and ATM.

distances and mine depths. Results are presented in Fig. 6 and Fig. 7, respectively.

As shown in Figs. 6 and 7, the net counts clearly decrease as the stand-off distance or the mine burial depth is increased, with optimum detection for a stand-off distance and a burial depth of 2 cm.

At this point, the complete ^{252}Cf–^{3}He assembly with optimized reflector and shields was scanned alternatively across the centers of both APM and ATM, when buried at 2 cm depth. The results were compared to those obtained when only ^{252}Cf–^{3}He assembly was used, without reflector or shields.

As it is seen in Figs. 8 and 9 the maximum net counts are always observed when the ^{252}Cf–^{3}He assembly passes over the center of the dummy landmines. The results shown in Figs. 8 and 9 clearly confirm that our empirically optimized shield increases effectively the net counts for both APM and ATM by about 167% and 121%, respectively.

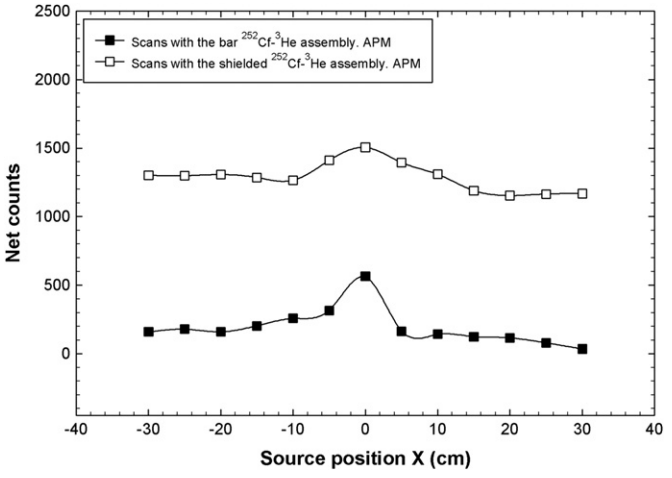

Fig. 8. Scans with shielded and bar ^{252}Cf–^{3}He assembly across the center of APM.

4. Monte Carlo simulations

4.1. The simulated geometry

Monte Carlo calculations were carried out to simulate the performance of the current detection system when a ^{252}Cf source of 10^4 s^{-1} is employed with an acquisition time similar to that of experimental work (1200 s). The obtained net signals were compared to those of experimental ones. To reduce the acquisition time, a ^{252}Cf source of 10^7 s^{-1} and 10^6 s^{-1} was employed with the current and an optimized geometry, respectively, for a duration of 100 s. The simulations were performed using the

Monte Carlo radiation transport code MCNP5, as described by the X-5 Monte Carlo Team (2003).

A point isotropic source was used with the neutron energy distribution characteristic of a ^{252}Cf source. A ^{3}He detector of the same dimensions as that used in the experimental work was employed to record only the number of back-scattered thermal neutrons detected by the ^{3}He(n,p)H^{3} reaction. A schematic representation of the simulated geometry is shown in Fig. 10. The APM and ATM were simulated by TNT of densities 1.18 g/cm^3 and 1.6 g/cm^3, respectively.

The APM was in a form of a cylinder of 7 cm diameter and 3 cm height, sealed in a cylindrical high density polyethylene (HDP) of density 0.955 g/cm^3, 8 cm diameter and 0.5 cm thick, while the ATM mine material was simulated by a cylinder of 18 cm diameter and 6 cm height sealed in a cylindrical (HDP) of 8 cm diameter and 0.5 cm thick.

Both mines were buried at 2 cm depth in a sandy soil bed with the same dimensions as that of the experiment. The soil composition was taken from Palomba et al. (2003) with the density set at a value of 1.5 g/cm^3.

The first two layers of the shield of boric acid and carbon were simulated with the same dimensions as in the experiment while the gadolinium oxide layer was lengthened to be of 40 cm length, to completely cover the detector.

For simplicity, all three layers forming the shield were simulated as bar materials without containers. The assumed elemental composition of TNT, polyethylene, boric acid and gadolinium oxide as modeled in the MCNP simulations is given in Table 1.

As a first task, we have explored the neutron dose to the operator at 100 cm above the shield. The annual dose limit for a radiological worker is 20 mSv (Datema et al., 2002). The dose rates for the simulated bar ^{252}Cf source in our shielded ^{252}Cf–^{3}He assembly with intensities of 10^4 s^{-1} and 10^7 s^{-1} were approximately 0.0002 mSv/h and 0.06 mSv/h, respectively, which are mainly due to the emitted neutrons.

In case of the ^{252}Cf source of 10^4 s^{-1}, if our device is used for 1000 h/year, a neutron dose of 0.2 mSv is expected, which suggests that our device operating time may reach 100,000 h which suits the requirements of the dose limit within the present application, while the operating time in case of the ^{252}Cf source of 10^7 s^{-1} is limited by only 330 h before reaching the annual dose limit when used as a hand-held manned detection system. The dose problem suggests the use of our system in the latter case as a robotic unmanned detection system.

The simulated detection system was then used to scan both APM and ATM with a scanning time of 1200 s and 100 s for the ^{252}Cf sources of 10^4 s^{-1} and 10^7 s^{-1}, respectively, at each measurement point. The results are presented in Figs. 11 and 12.

Compared to the experimental results for the shielded ^{252}Cf–^{3}He assembly presented in Figs. 8 and 9, the net counts in Fig. 11 are greater by a factor of about 2 and 5 for APM and ATM, respectively. This may be attributed to the presence of the aluminum box in measurements which may react with the

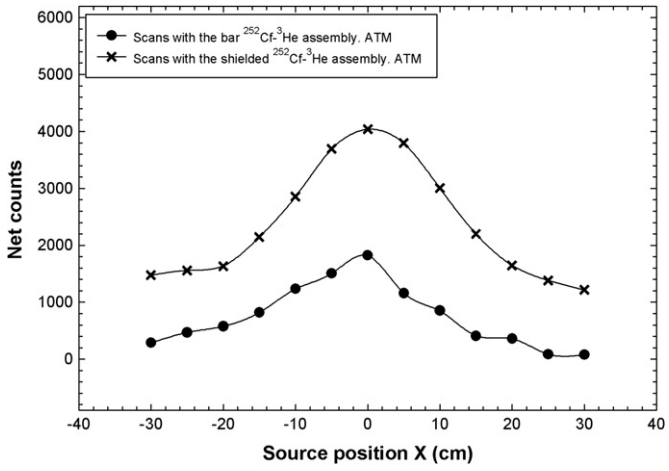

Fig. 9. Scans with shielded and bar ^{252}Cf–^{3}He assembly across the center of ATM.

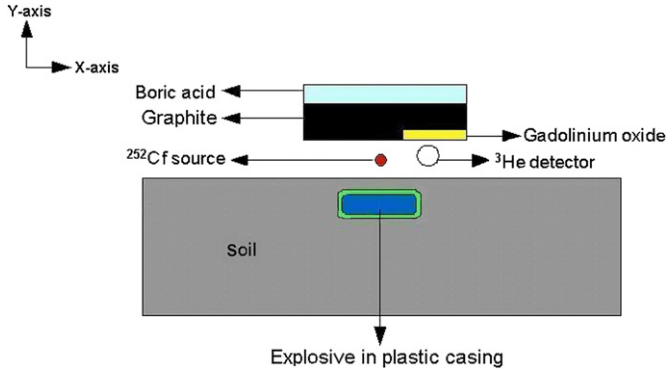

Fig. 10. Geometry as modeled in the MCNP simulations for the detection system.

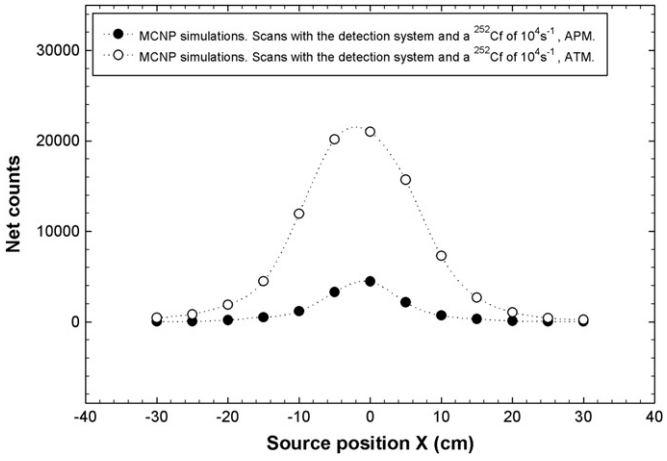

Fig. 11. MCNP results for scans with the detection system across the center of both APM and ATM with a ^{252}Cf source of 10^4 s^{-1}.

Table 1
Composition of TNT, polyethylene, boric acid and gadolinium oxide (rounded off) as modeled in the MCNP simulations.

Material/Density (g/cm^3)	Mass fractions													
	H	^{10}B	^{11}B	C	N	O	Si	Al	Fe	Ca	K	Na	Mg	Gd
TNT 1.18	**0.238**			**0.333**	**0.143**	**0.286**								
Polyethylene 0.955	**0.143**			**0.857**										
Boric acid 1.47	**0.018**	**0.035**	**0.155**			**0.792**								
Gadolinium oxide 7.41						**0.132**								**0.868**

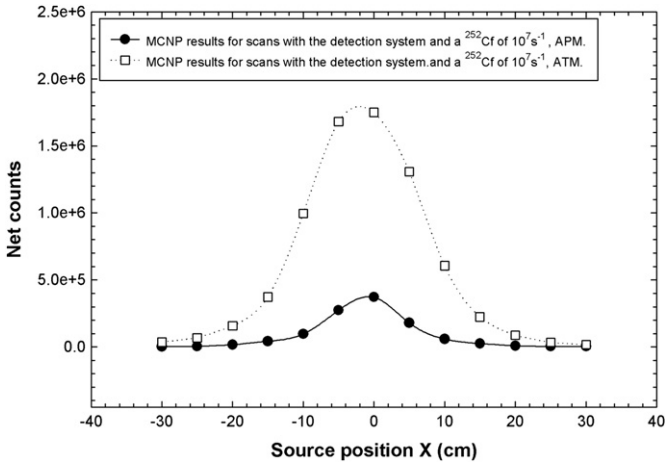

Fig. 12. MCNP results for scans with the detection system across the center of both APM and ATM with a ^{252}Cf source of 10^7 s^{-1}.

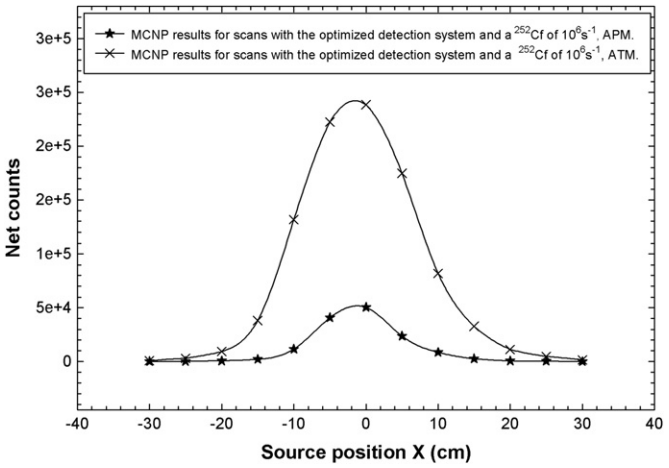

Fig. 14. MCNP results for scans with the optimized detection system across the center of both APM and ATM with a ^{252}Cf source of 10^6 s^{-1}.

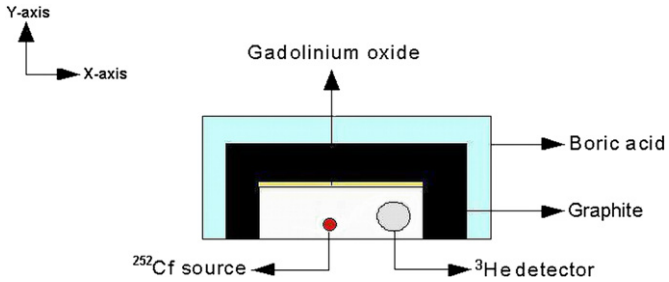

Fig. 13. Geometry as modeled in the MCNP simulations for the optimized detection system.

neutrons reflected back from carbon reducing the number of neutrons directed towards the soil.

On the other hand, the point isotropic ^{252}Cf source used in the simulations may contribute to the increase of net counts. As shown in Figs. 11 and 12, the net signal peaks for both mines occur when the system passes over the landmine and the net counts increase approximately by a factor of 4 for ATM compared to that of APM.

4.2. The geometry for a future prototype

The source intensity that may be used in the current detection system in view of a future prototype device needs to be as low as possible due to the radiation dose for the operator and sufficient to detect the landmine and reduce the acquisition time. The lower limit for the source intensity is defined by factors that include the acquisition time or scanning speed, net signal due to the buried explosive, soil moisture, mine depth, etc. In view of these facts and the dose rate recorded for the simulated detection system, a ^{252}Cf source producing 10^6 s^{-1} was employed and the design of the shield was optimized as a cube-like shape with two edges. A schematic representation of the optimized geometry is shown in Fig. 13. The edges were added to maximize the neutron flux density toward the buried target and to enhance the performance of boric acid layer in reducing the dose rate for the operator. The shield consists of four cube-like shapes centered around the source position.

The first is of 2 cm thick, 9 cm height and 40 cm length, representing the boric acid layer, while the second is of 3 cm thick, 7 cm height and the same length, representing the carbon reflector. The third is of dimensions 40 cm × 14 cm × 0.5 cm representing the gadolinium oxide layer, while the fourth is the cavity in which the ^{252}Cf source and the ^{3}He detector were located with the same geometry as that of the experiment.

The dose rate for the simulated bar ^{252}Cf source in our optimized detection system with intensity of 10^6 s^{-1} was approximately 0.01 mSv/h at a distance of 100 cm above the shield. Compared to the operating time when a ^{252}Cf source of 10^7 s^{-1} is used, if our optimized device is used for 1000 h/year, a neutron dose of 10 mSv is expected, which extends the operating time to 2000 h/year before the annual dose limit is reached.

In view of this fact, our optimized detection system with a ^{252}Cf source of 10^6 s^{-1} is clearly suitable for a hand-held manned detection system.

Simulations were performed using the optimized shielded (^{252}Cf–^{3}He) assembly to scan over the center of both APM and ATM at a duration of 100 s. The results are shown in Fig. 14.

Compared to the MCNP scanning results for the detection system with 10^7 s^{-1} ^{252}Cf source, the net signal for both APM and ATM drops approximately by a factor of 7.

On the other hand, our optimized detection system has significantly minimized the dose rate for the operator by about 80% and increased the operating time by about 500%. Highest net signal was observed when the system passes over the landmine.

5. Conclusion

The working principle of landmine detection using neutron back-scattering has been confirmed. The performance of a suitable shielded (^{252}Cf–^{3}He) assembly was investigated experimentally in the presence of a ^{252}Cf source producing about 10^4 s^{-1} and by means of MCNP simulations in the presence of a ^{252}Cf source producing 10^4 s^{-1}, 10^6 s^{-1} and 10^7 s^{-1}. The optimal configuration of the empirically optimized shield was found to be 2 cm of boric acid, 4 cm carbon and 0.5 cm gadolinium oxide.

The experiments demonstrated that the proposed shield has significantly improved the net signal due to the buried two dummy landmines with an excess net signal for ATM.

The shielded (^{252}Cf–^{3}He) assembly was simulated in the presence of a ^{252}Cf source producing 10^4 s^{-1}. The simulated source showed higher net signals compared to the experimental ones for the same operating time of 1200 s. To reduce the operating time, a stronger ^{252}Cf source producing 10^7 s^{-1} was employed and a duration of 100 s was considered. The ^{252}Cf source of 10^7 s^{-1} has significantly increased the net counts due to

the buried explosive, reduced the acquisition time and recorded best results when the ^{252}Cf source was at 2 cm above the soil and landmine at 2 cm burial depth.

But in view of the annual permissible dose limit for operators classified as radiation workers of 20 mSv, the operating time of our simulated detection system when used as a hand-held manned detection system is limited to only 330 h/year since it produces a dose rate of about 0.06 mSv/h. Otherwise it can be integrated to a robotic system and used as an unmanned detection system with no operating time limitations.

Based on the results of the experiments and simulations described in this work, a ^{252}Cf source producing 10^6 s^{-1} was also employed and the shield was optimized in view of a future prototype with lower reflector thickness and extra two edges.

With respect to the net signals due to the buried explosives, our optimized detection system has positively identified the two dummy landmines at a duration of 100 s with an acceptable contrast, while for the dose rate, the simulations confirmed the superiority of our future prototype over the simulated detection system with a ^{252}Cf of 10^7 s^{-1}.

The results showed that the neutron back-scattering method is sensitive to shield configuration, source intensity, stand-off distance and mine depth. The small size of APM and its low hydrogen content complicate its detection and make it more challenging compared to ATM.

Acknowledgments

Special debt is owed to the Dipartimento di Fisica degli Universita di Padova for supporting and hosting this work in collaboration with the ICTP-IAEA **S**andwich **T**raining **E**ducational **P**rogram (STEP). The authors are grateful to Mrs. Antonietta Donzella at Universita' di Brescia, Facolta' di Ingegneria, for useful discussions concerning MCNP simulations.

References

Bom, V.R., Datema, C.P., Van Ejik, C.W.E., 2004. The status of the Delft University Neutron Backscatter landmine Detector (DUNBLAD). Appl. Radiat. Isot. 61, 21–25.

Borgonovi, G.M., Ginaven, R.O., Orphan, V.J., 2000. Landmines and Unexploded Ordnance Detection, in a Remotely Controlled Multi-Sensor Platform for Humanitarian Demining. Report for the Advisory Group meeting held 3–7 April 2000 at the IAEA Headquarters. Vienna, Austria, IAEA Publication IAEA/PS/AG-1093.

Brooks, F.D., Drosg, M., 2005. The HYDAD-D antipersonnel landmine detector. Appl. Radiat. Isot. 63, 565–574.

Brooks, F.D., Drosg, M., Buffer, A., Allie, M.S., 2004. Detection of anti-personnel landmines by neutron scattering and attenuation. Appl. Radiat. Isot. 61, 27–34.

Cinausero, M., Lunardon, M., Nebbia, G., Pesente, S., Viesti, G., Filippini, V., 2004. Development of a thermal neutron sensor for Humanitarian Demining. Appl. Radiat. Isot. 61, 59–66.

Cousins, T., Jones, T.A., Brisson, J.R., McFee, J.E., Jamieson, T.J., Waller, E.J., Lemay, F.J., Ing, H., Clifford, E.T., Selkirk, E.B., 1998. The development of a thermal neutron activation (TNA) system as a confirmatory non-metallic landmine detector. Radioanal. Nucl. Chem. 235, 53–58.

Csikai, J., Doczi, R., Kiraly, B., 2004. Investigations on landmine detection by neutron-based techniques. Appl. Radiat. Isot. 61, 11–20.

Datema, C.P., Bom, V.R., Van Eijk, C.W.E., 2000. Landmine detection with the neutron backscattering method. IEEE Nucl. Sci. Conf. Rec. 1, 5111–5114.

Datema, C.P., Bom, V.R., Van Eijk, C.W.E., 2002. Experimental results and Monte Carlo simulations of a landmine localization device using the neutron backscattering method. Nucl. Instrum. Methods A 488, 441–450.

D'Mellow, B., Thomas, D.J., Joyce, M.J., Kolkowski, P., Roberts, N.J., Monk, S.D., 2007. The replacement of cadmium as a thermal neutron filter. Nucl. Instrum. Methods A 577, 690–695.

Hussein, E.M.A., Waller, E.J., 2000. Landmine detection: the problem and the challenge. Appl. Radiat. Isot. 53, 557–563.

Kuznetsov, A.V., Evsenin, A.V., Gorshkov, I.Yu., Osetrov, O.I., Vakhtin, D.N., 2004. Detection of buried explosives using portable neutron sources with nanosecond timing. Appl. Radiat. Isot. 61, 51–57.

Kiraly, B., Olah, L., Csikai, J., 2001. Neutron-based techniques for detection of explosives and drugs. Radiat. Phys. Chem. 61, 781–784.

Knoll, G.F., 1989. Radiation Detection and Measurement, second ed. Wiley, New York.

Lunardon, M., Nebbia, G., Pesente, S., Viesti, G., Barbui, M., Cinausero, M., D'Erasmo, G., Palomba, M., Pantaleo, A., Filippini, V., 2004. Detection of landmines using 14 MeV neutron tagged beams. Appl. Radiat. Isot. 61, 43–49.

McFee, J., Aitken, V., Chesney, R., Das, Y., Russel, K., 1998. A multi sensor, vehicle-mounted, teleoperated mine detector with data fusion. In: Proceedings of the 1998 Conference on Detection and Remediation Technologies For Mines and Minlike Targets III. Orlando, USA, pp. 1082–1093, (SPIE 3392).

Obhadas, J., Sudac, D., Nad, K., Valkovic, V., Nebbia, G., Viesti, G., 2004. The soil moisture and its relevance to landmine detection by neutron backscattering technique. Nucl. Instrum. Methods B 213, 445–451.

Palomba, M., D'Erasmo, G., Pantaleo, A., 2003. The Monte Carlo code CSSE for the simulation of realistic thermal neutron sensor devices for Humanitarian Demining. Nucl. Instrum. Methods A 498, 384–396.

Reines, F., Cowan, C.L., 1953. Phys. Rev. 92, 830.

Sieber, A.I. (Ed.), 1998. A.I. Proceeding of Demining Technologies. ICR Ispra 1998. Report EUR 18682 EN.

Vourvopoulos, G., Womble, P.C., 2001. Pulsed fast/thermal neutron analysis: a technique for explosives detection. Talanta 54, 459–468. (and references therein).

Viesti, G., Lunardon, M., Nebbia, G., Barbui, M., Cinausero, M., D'Erasmo, G., Palomba, M., Pantaleo, A., Obhođaš, J., Valkovic, V., 2006. The detection of landmines by neutron backscattering: exploring the limits of the technique. Appl. Radiat. Isot. 64, 706–716.

X-5 Monte Carlo Team, 2003. MCNP—A General Monte Carlo N-Particle Transport Code: Overview And Theory. Version 5. Los Alamos National Laboratory, April 24, 2003 (Revised 6/30/04).